Spin Magnetization in the Hall Effect Ground State of Bose-Einstein Condensates

Hugo Bencomo Martín
Universidad de La Laguna, Tenerife 38200, Spain

Antonio Muñoz Mateo
Departamento de Física, Universidad de La Laguna, La Laguna, Tenerife, Spain
(Dated: March 20, 2026)

I. INTRODUCTION

The probability current in non-relativistic quantum mechanics presents subtleties when spin is considered. In this case one has to use the Pauli equation, but then the probability current density is not well defined. It can only be derived without ambiguity from the Dirac equation [1, 2], and, in this way, an additional spin term arises in the non-relativistic limit. Although this term has null divergence, hence no contribution to the continuity equation, which might be the reason why it is often neglected, it can still lead to relevant physical effects, as it is the case for the quantum Hall effect [2]. The purpose of this work is to show that there is a non-zero contribution of the spin term in the current density of the ground state of both a non-interacting and an interacting Bose-Einstein condensate of neutral atoms that, subjected to synthetic gauge fields [3], simulate the integer quantum Hall effect. Our findings can be easily tested in current experiments with ultracold-gas systems.

In this work, we demonstrate both analytically and numerically the exact cancellation of the probability current in the bulk of a non-interacting BEC for a concrete spin polarization. Furthermore, we reveal that the introduction of a Gross-Pitaevskii (GP) repulsive interaction breaks the cancellation, leading to a macroscopic net current. Additionally, we verify the robustness of our model by recovering the classical Hall effect drift when an external electric field is applied. Finally, we study the interplay between the Hall effect drift and the GP interaction.

II. THEORETICAL FRAMEWORK

Within a mean-field framework, the Pauli equation for interacting spin-1/2 particles reads,

$$i\hbar\partial_t\,\chi = \frac{(\boldsymbol{\sigma}\cdot\hat{\mathbf{p}})^2}{2m}\,\chi + g|\chi|^2\chi, \tag{1}$$

where $\boldsymbol{\sigma} = \{\sigma_x, \sigma_y, \sigma_z\}$ is the vector of Pauli matrices, and the interparticle interaction strength $g = 4\pi\hbar^2 a/m$ is assumed to be proportional to the scattering length a. Equation (1) can be obtained in the linear regime, $g = 0$, from the non-relativistic limit of the Dirac equation (see Appendix A). There, the Pauli spinor χ is the *large* component of the Dirac field $[\chi\,\phi]^T$, whose *small* component $\phi \approx \boldsymbol{\sigma}\cdot\hat{\mathbf{p}}\,\chi\,/2mc$, where c is the speed of light, provides the relativistic corrections. Analogously, starting from the Dirac current density $\mathbf{J}_{\text{Dirac}} = c\left(\chi^\dagger\,\boldsymbol{\sigma}\,\phi + \phi^\dagger\,\boldsymbol{\sigma}\,\chi\right)$ (See Sakurai [4]), one obtains the corresponding Pauli current density

$$\mathbf{J} \approx \chi^\dagger\,\boldsymbol{\sigma}\,\frac{\boldsymbol{\sigma}\cdot\hat{\mathbf{p}}}{2m}\chi + \chi^\dagger\frac{(\boldsymbol{\sigma}\cdot\hat{\mathbf{p}})^\dagger}{2m}\boldsymbol{\sigma}\,\chi \tag{2}$$

$$= \frac{1}{m}\,\mathrm{Re}\{\chi^\dagger\,\hat{\mathbf{p}}\,\chi\} + \frac{\hbar}{2m}\,\nabla\times(\chi^\dagger\boldsymbol{\sigma}\chi). \tag{3}$$

As anticipated, the additional spin term $\mathbf{J}_\sigma = \nabla\times\mathbf{s}\,/m$, where $\mathbf{s} = (\hbar/2)\chi^\dagger\boldsymbol{\sigma}\chi$ is the spin-density vector, does not contribute to the continuity equation $\partial_t\chi + \boldsymbol{\nabla}\cdot\mathbf{J} = 0$, since $\boldsymbol{\nabla}\cdot(\nabla\times\mathbf{J}_\sigma) = 0$, and can be understood as a spin or magnetization current density.

For a system of electrically charged particles in the presence of an electromagnetic field, assuming a minimal coupling, Eqs. (1) and (3) remain valid by making the substitutions $\hat{\mathbf{p}} \to \hat{\boldsymbol{\pi}} = \hat{\mathbf{p}} - q\mathbf{A}$ and $i\hbar\partial_t \to i\hbar\partial_t - qV$, where $\{V, \mathbf{A}\}$ are the electromagnetic potentials. In order to study a Hall system, where the motion takes place within the $x-y$ plane, a constant, perpendicular magnetic field B_z, with z-direction, is considered along with an in-plane, constant electric field $-E_x$, with negative x-direction. We write the electromagnetic potentials in the so-called Landau gauge

$$V = E_x\,x, \quad \mathbf{A} = (0, B_z\,x, 0),$$

and, as a result, the Pauli Hamiltonian in Eq. (1) becomes

$$\hat{H} = \frac{\hat{p}_x^2 + (\hat{p}_y - qB_z x)^2}{2m} - \frac{q\hbar}{2m}\,\sigma_z\,B_z + q\,E_x\,x + g|\chi|^2, \tag{4}$$

where we have not included the dependence on the $z-$coordinate, assuming that the system is frozen in its ground state along this direction.

Since $[\hat{H}, \sigma_z] = 0$, and $[\hat{H}, \hat{p}_y] = 0$ if $|\chi|^2$ does not depend on the $y-$coordinate, one can search for solutions to Eq. (1) with the functional form

$$\chi(x, y, t) = \begin{pmatrix} c_\uparrow \\ c_\downarrow \end{pmatrix}\chi(x)\,\frac{1}{\sqrt{L_y}}e^{i(ky-\mu t/\hbar)}, \tag{5}$$

where L_y is the system length along y, and $[c_\uparrow\,c_\downarrow]^T = \{[1\,0]^T, [0\,1]^T\}$ are the eigenvectors of the σ_z operator with eigenvalues $\sigma = \pm 1$, respectively.

A. The non-interacting Hall system

It is insightful to start from the non-interacting limit, $g = 0$, where the analytical solutions to the eigenvalue equation for $\chi(x)$ are known. From the direct substitution of (5) in Eq. (1), one gets

$$\left[\frac{\hat{p}_x^2}{2m} + \frac{m\omega_B^2(x-x_k)^2}{2} + \mathcal{E}_k - \frac{\hbar\sigma}{2}\omega_B\right]\chi(x) = \mu\chi(x), \tag{6}$$

where we have defined

$$\omega_B = \frac{|q|B_z}{m}, \quad x_k = \frac{\hbar k}{qB_z} - \frac{mE_x}{qB_z^2}. \quad \mathcal{E}_k = \frac{\hbar k E_x}{B_z} - \frac{mE_x^2}{2B_z^2}. \tag{7}$$

The solutions to Eq. (6) are (real) Hermite functions [5] $\chi(x) = \mathcal{H}_n[(x-x_k)/\ell_B]\exp\left[-(x-x_k)^2/2\ell_B^2\right]$, product of a Hermite polynomial $\mathcal{H}_n$ of order n times a gaussian of width $\ell_B = \sqrt{\hbar/m\omega_B}$, and give rise to the appearance of the celebrated Landau levels [6] in the energy spectrum of the Hamiltonian Eq. (4),

$$E_{n,\sigma,k} = \hbar\omega_B\left(n + \frac{1-\sigma}{2}\right) + \mathcal{E}_k. \tag{8}$$

labeled by the excitation number $n = 0, 1, 2, \ldots$ of a harmonic oscillator characterized by the cyclotron frequency ω_B. The total eigenenergy depends also on spin, labeled by σ, and, due to the presence of the electric field, on the momentum $\hbar k$ along the $y-$direction. For generic stationary eigenstates $\chi_{n,\sigma,k}(x,y)$ the Pauli probability current Eq. (3) gives a Hall current

$$\mathbf{J} = |\chi|^2\left(0, \frac{\hbar k - m\omega_B\, x}{m} - \sigma\,\frac{\hbar}{2m}\,\partial_x \ln|\chi|^2, 0\right), \tag{9}$$

along the $y-$direction, perpendicular to the direction of the applied electric field, with a spin current contribution $J_{y_\sigma} = -\sigma\,\hbar\,\partial_x|\chi|^2/2m$ of opposite sign for the two spin components. By using the explicit form of the eigenfunctions, the spin current density becomes

$$J_{y_\sigma} = \frac{\sigma\, e^{-\tilde{x}^2}}{L_y\ell_B}\mathcal{H}_n(\tilde{x})^2\,\tilde{x}\,\omega_B\ell_B, \tag{10}$$

where we have set $\tilde{x} = (x - x_k)/\ell_B$, while the orbital contribution is

$$J_y - J_{y_\sigma} = \frac{e^{-\tilde{x}^2}}{L_y\ell_B}\mathcal{H}_n(\tilde{x})^2\,\frac{\hbar k - m\omega_B x}{m}; \tag{11}$$

their combination produces the total current density

$$J_y = \frac{e^{-\tilde{x}^2}}{L_y\ell_B}\mathcal{H}_n(\tilde{x})^2\left[(\sigma-1)\tilde{x}\,\omega_B\ell_B + \frac{E_x}{B_z}\right]. \tag{12}$$

In particular, for the lowest Landau level, $n = 0$, the spin polarized ($\sigma = 1$) eigenstates

$$\chi_{0,1,k}(x,y,t) = \begin{pmatrix}1\\0\end{pmatrix}\frac{e^{-\tilde{x}^2/2}}{\sqrt{L_y\ell_B\sqrt{\pi}}}\,e^{i(ky - \mathcal{E}_k t/\hbar)}; \tag{13}$$

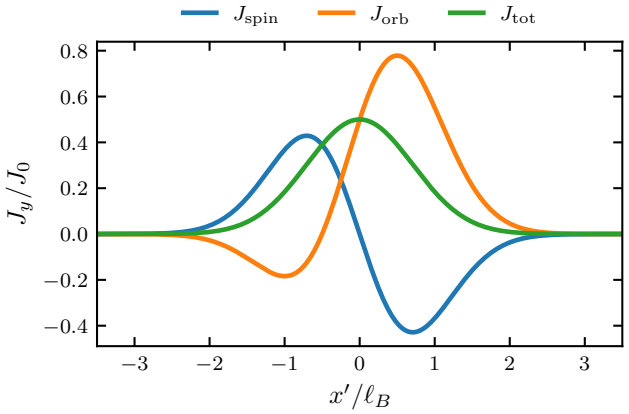

FIG. 1. Components of the Pauli probability current density in the lowest Landau level ($n = 0$) in a system with $E_x/B_z = 0.5\,\omega_B\ell_B$ as functions of the non-dimensional coordinate $\tilde{x} = (x - x_k)/\ell_B$. As can be seen in Eq. (12), the orbital and spin contributions that are odd in $\tilde{x}$ cancel locally. Currents are represented in units of $J_0 = e^{-\tilde{x}^2}\,\omega_B\ell_B/(L_y\ell_B\sqrt{\pi})$.

have energy eigenvalue $\mathcal{E}_k$, and current density

$$J_y = |\chi_{0,1,k}|^2\,\frac{E_x}{B_z} = \frac{e^{-\tilde{x}^2}}{L_y\ell_B\sqrt{\pi}}\,\frac{E_x}{B_z}. \tag{14}$$

which is proportional to the *drift* velocity $v_d = E_x/B_z$. Figure 1 represents this current density in a system with $v_d = 0.5\,\omega_B\ell_B$. As can be seen, the spin-current term does not vanish and is odd in the shifted $\tilde{x}-$coordinate; after adding the orbital term, the total current density shows an even gaussian profile.

B. The interacting Hall system

Further analytical insight can be obtained by considering the regime dominated by interactions, where $\mu \gg \hbar\omega_B$. In this case, the Thomas-Fermi ansatz

$$\chi_{TF}(x) = \begin{pmatrix}1\\0\end{pmatrix}\sqrt{\frac{\mu_{eff} - \frac{1}{2}m\omega_B^2(x-x_k)^2}{g}}, \tag{15}$$

for $\chi \geq 0$ and $\chi = 0$ otherwise, where $\mu_{eff} = \mu - \mathcal{E}_k + \hbar\omega_B/2$, approximates the ground state by neglecting the kinetic energy in the $x-$direction, along which the condensate extension, $x \in [x_k - R_{TF}, x_k + R_{TF}]$, is determined by the Thomas-Fermi radius $R_{TF} = \sqrt{2\mu_{eff}/m}\,/\omega_B$. In contrast with the linear case of Eq. (14), the current density

$$J_y = -\left(\chi_{TF}^2 + \frac{\hbar\omega_B}{g}\right)(x - x_k)\omega_B + \chi_{TF}^2\,\frac{E_x}{B_z}, \tag{16}$$

takes nonzero values in the absence of electric field. Enforcing normalization $\int \chi_{TF}^2 dxdy = N$ to the number of

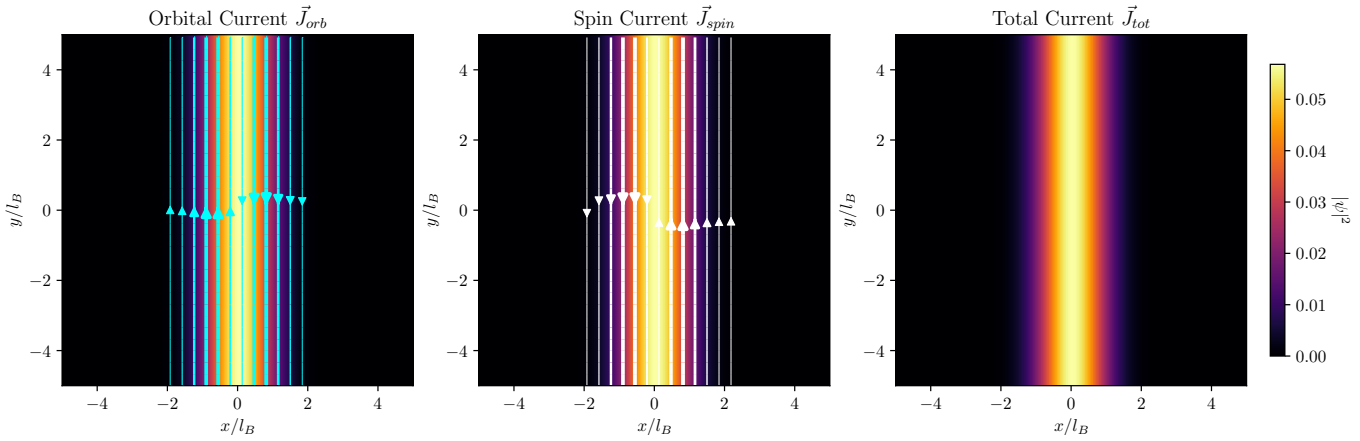

FIG. 2. Two-dimensional representation of the probability current densities for the non-interacting ground state ($g = 0$) in the Landau gauge. From left to right: orbital current $\vec{J}_{orb}$, spin current $\vec{J}_{spin}$, and total current $\vec{J}_{tot}$. The local current magnitude is encoded in the thickness of the streamlines, overlaid on the probability density $|\psi|^2$ background. The exact local cancellation in the bulk of the condensate is clearly visible (right panel).

particles N in the condensate, one obtains the chemical potential as a function of the electromagnetic fields,

$$\mu = \frac{\hbar\omega_B}{2} + \frac{1}{\omega_B}\left(\frac{\hbar k}{m} - \frac{E_x}{B_z}\right) + \left(\frac{3\sqrt{m}\,\omega_B g N}{4\sqrt{2}L_y}\right)^{2/3}. \tag{17}$$

The Thomas-Fermi ansatz, through Eq. (16), demonstrates the presence of high, counter-propagating currents around the center lines $x = x_k$ for increasing values of the magnetic field, which, as in classical fluids, could lead to instabilities of the Kelvin-Helmholtz type. As a result, the emergence of quantum vortices is expected beyond a particle current threshold...

III. NUMERICAL RESULTS

As explained before, because of the new term we have to resort to numerical methods. The first step, is to implement a time-imaginary script that can evolve an arbitrary initial state into the ground state (see [7]). To simulate the topology described in Appendix B, Fourier Fast Transform (FFT) are used, which assume periodic boundary conditions to deal efficiently with derivative terms. In the y direction we assumed periodic boundary conditions, so it is consistent. Nevertheless, in the x direction we assumed infinite walls (confined system). Therefore, a new potential term has to be introduced in order to confine the system in the x direction. The script used, implements a potential of the form

$$V_{well} = V_0 \times \left[1 + 9 \cdot tanh(|x| - 0.75 \cdot x_{max})\right] \tag{18}$$

with $V_0 = 9\hbar\omega_B$, and $x_{max} = L_x/1.5$. This potential ensures there is no conflict with our gauge and the FFT. With the numerical ground state, it is possible to compute the probability density currents for this state. This does not require the introduction of anything new, it is just a matter of implementing the equations. The result obtained for imaginary time evolution in the non interacting case (g = 0) and zero electric field $E = 0$ is depicted in Fig. 2. As a heat map, the probability density ($|\psi|^2$) is plotted in 2D. On top, the currents are represented for three different terms. On the left we have the orbital term, which only flows in the y direction; in the middle we have the spin term contribution, which in this case is exactly equal to the orbital contribution but with opposite direction; on the right we have the total which is the addition of the other two terms, that cancel out to give a null contribution.
A transversal representation of Fig. 2 can be performed for visual clarity, and in order to compare with the theoretical results derived in II A (figure 1) We see clearly in the top-left panel of Fig. 4 the cancellation of both terms, accordingly to the derived expression for the total current (14).

A. Adding Interaction: Breaking the topological cancellation

If the Gross-Pitaevskii term is activated, for instance a strong repulsion term with $g = 50$, we expect the same functional form of the ground state density only with a thicker distribution. Using the same script as before, we can compute the ground state for this case (see heatmap of Fig. 3). At first glance, one might expect the total current to perfectly cancel out, just as in the non-interacting case. Nevertheless, when interaction g = 50 is added, a total non-zero current emerges. As the density profile broadens and the top flattens, the spatial gradients diminish. Consequently the spin term weakens (10), meanwhile

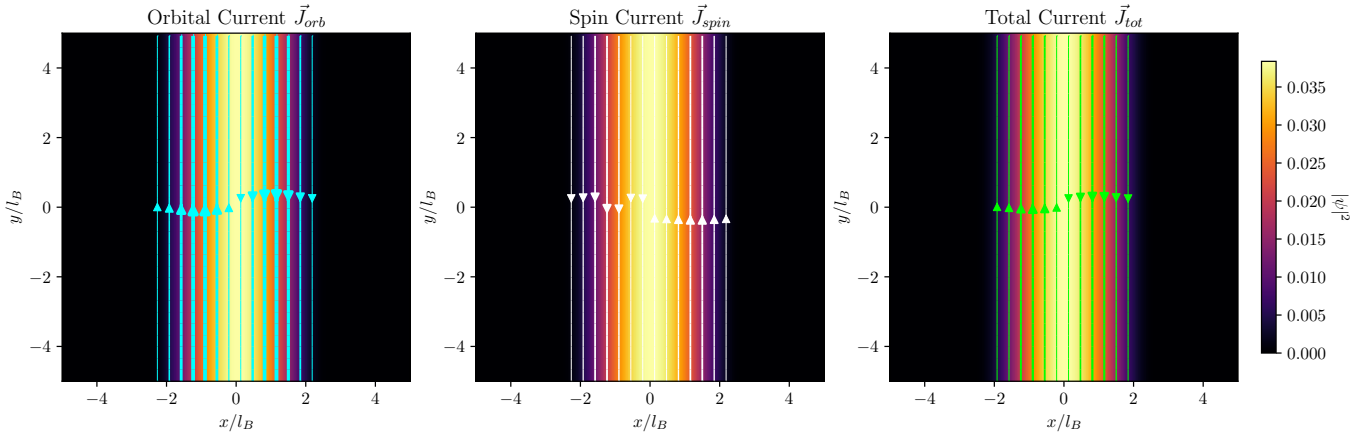

FIG. 3. Two-dimensional representation of the probability current densities for the interacting ground state ($g = 50$) in the Landau gauge. From left to right: orbital current $\vec{J}_{orb}$, spin current $\vec{J}_{spin}$, and total current $\vec{J}_{tot}$. Unlike the non-interacting case, the flattening of the density profile weakens the spin current. As a result, the exact local cancellation in the bulk is broken, giving rise to a visible net total current (green streamlines in the right panel) flowing through the center of the condensate.

the gauge part of the orbital term does not change (only the wave-function). Therefore the spin term is no longer able to fully offset the orbital term, breaking the topological cancellation. This behavior is clearly illustrated in Fig. 3 As before, it is possible to do a transversal representation of the current. Where the current in the y direction is plotted against x. In the top-right panel of Fig. 4 it is possible to see clearly the weakening of the spin term (blue), and the appearance of a total current (green).

B. Macroscopic Transport under an External Electric Field

To complete our analysis and verify the macroscopic transport properties of the system, we study the condensate under the influence of an external in-plane electric field $\vec{E} = -E\hat{x}$. In this scenario, classical electromagnetism predicts a uniform $\vec{E} \times \vec{B}$ Hall drift in the y-direction.

From our analytical framework, we demonstrated in section A that for a non-interacting gas ($g = 0$) with proper spin polarization, the spin current perfectly cancels the orbital current. This exact cancellation leaves only a net macroscopic flow proportional to the drift velocity $v_d = E/B$. To verify this, we run our simulation setting $E = 0.5$ and $g = 0$.

First, the external electric field alters the effective potential of the system, shifting the equilibrium position of the harmonic trap to $x_0 = -mE/qB^2$. In our dimensionless units, this corresponds to a shift of the condensate center to $x_0 = -0.5l_B$, which is perfectly captured by the shift of the Gaussian shown in the bottom-left panel of Fig. 4. More importantly, the transport properties strictly follow the topological cancellation. As shown in the bottom-left panel of Fig. 4, the spin and orbital currents still mirror each other to cancel the shear, but their sum is no longer zero. Instead, the total current yields a net macroscopic flow profile that perfectly matches the density distribution, confirming the exact analytical prediction of the Hall drift, which was depicted in Fig. 1. Note that the current orientation is inverted with respect to Fig. 1 due to the opposite sign of the charge and spin polarization used in the analytical derivation. We also see that the bottom-left panel of Fig. 4 is shifted, this is because it is plotted against x/ℓ_B, and not $\tilde{x}/\ell_B$.

When we combine interaction (g = 50) with an electric field ($E = 0.5$). The wave-function broadens, and is also shifted because of the field dependence of equilibrium position of the harmonic trap ($x_0 = -mE/qB^2$). The drift velocity of the bulk is still in the y direction. Nevertheless, border currents appear with opposite direction to that of the bulk. For this groundstate, we see in the bottom-right panel of Fig. 4 that overall, the orbital and spin term have the same structures. Nevertheless, because of the interaction the spin term weakens with respect to the orbital one. And because of the electric field, it is noticeable that the orbital current mostly concentrates in the left border. Both terms add up to give a bulk current in the y direction. Additionally, smaller border currents are formed, which can be seen in the bottom-right panel of Fig. 4.

IV. CONCLUSIONS

In this work, we have thoroughly investigated the current density of a Bose-Einstein Condensate under synthetic gauge fields, which simulate the integer quantum hall effect. First of all we have seen the contribution of the spin term in the ground state of the Hall effect. Then, how in specific settings of the ground state the spin term

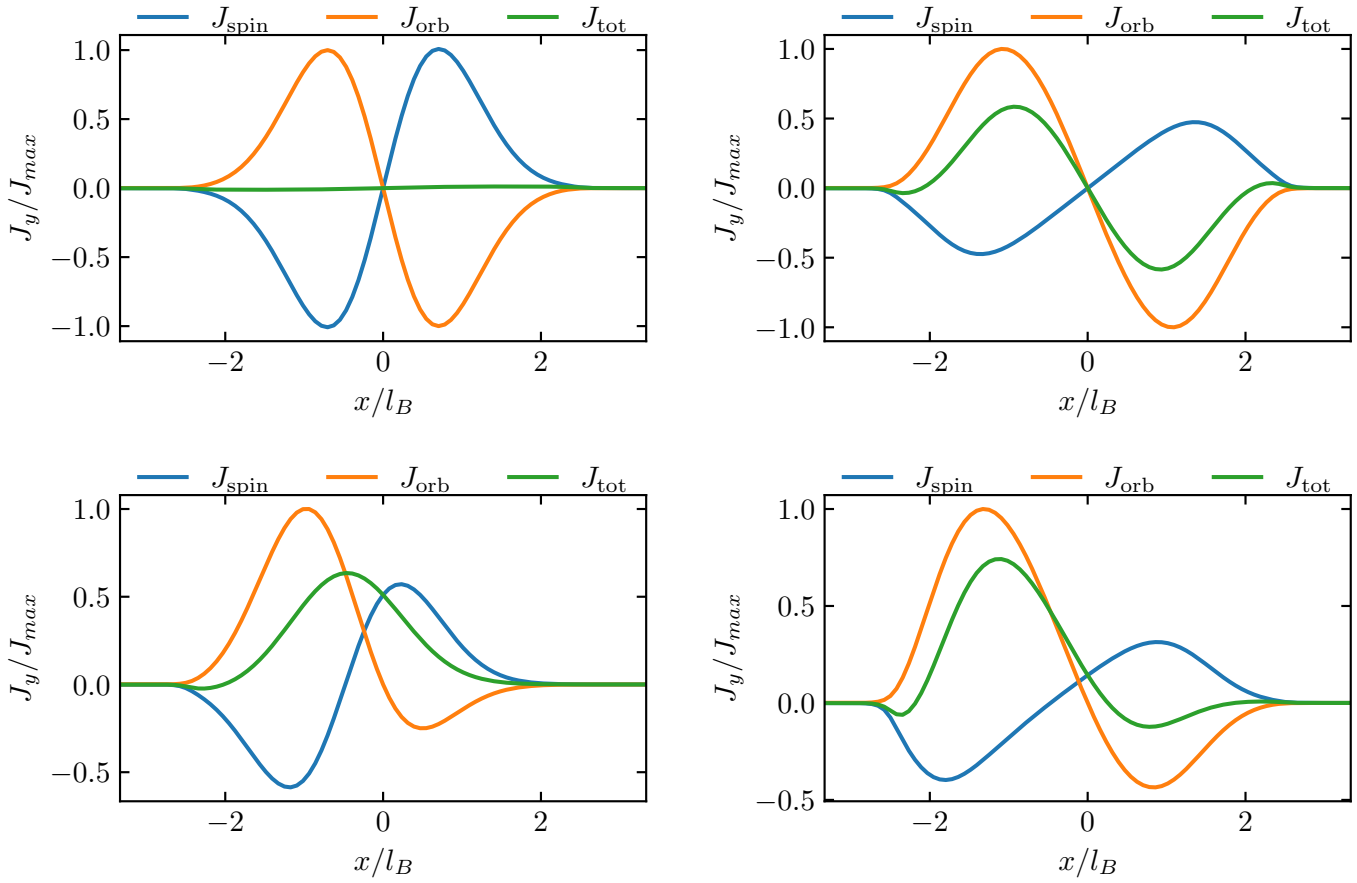

FIG. 4. Transverse profile of the probability current densities for the four regimes studied in this work. **Top-left:** Non-interacting gas ($g = 0$) at rest ($E = 0$), showing the perfect local cancellation of the spin (blue) and orbital (orange) shear components, leaving a null total current (green) in the bulk. **Top-right:** Interacting gas ($g = 50$) at rest. The density flattening weakens the spin term, breaking the cancellation and inducing a net bulk current. **Bottom-left:** Non-interacting gas under an applied electric field ($E = 0.5$). The cancellation perfectly holds for the shear terms, exposing the macroscopic $\vec{E} \times \vec{B}$ Hall drift. **Bottom-right:** Interacting gas under an electric field, demonstrating the interplay between the classical Hall drift (shifted peak) and the interaction-driven breakdown of the topological shielding (broadened profile).

sets off the orbital term to give a null total current. An insight the simulations have shown, is how activating a repulsive interaction between the components of the BEC weakens the spin term, as a result a total contribution arises. Finally, the simulations have proven that when an electric field is activated, the bulk shifts in the field direction, and a drift velocity appears in the $E \times B$ direction, in accordance with classical Hall drift. For the interacting regime, the current profile shows an intricate combination of the field-induced shift and the interaction-driven spin term weakening. These results not only resolve theoretical ambiguities posed by Pauli spin current but also open new avenues for experimental observation. The net bulk current predicted in the interacting regime could be readily measured in ultracold-gas setups, offering a novel tool to probe quantum macroscopic transport and topological properties in tunable quantum fluids. As well as posing a prospective new method to measure the interaction intensity g in these ultracold-gas experiments, through the measurement of currents.

Appendix A: From Dirac to Pauli equation

The Dirac Hamiltonian takes the compact form [8]

$$\hat{H}_{\text{Dirac}} = c\,\vec{\alpha}\cdot\hat{p} + \beta\, mc^2, \tag{A1}$$

in the representation where

$$\vec{\alpha} = \begin{pmatrix} 0 & \vec{\sigma} \\ \vec{\sigma} & 0 \end{pmatrix}. \qquad \beta = \begin{pmatrix} \hat{\mathbb{1}}_{2\times2} & 0 \\ 0 & -\hat{\mathbb{1}}_{2\times2} \end{pmatrix}, \tag{A2}$$

From Eq. (A1), and by writing the Dirac field in terms of its two-component spinors $[\chi\,\phi]^T$, one obtains the two coupled equations of motion

$$i\hbar\,\partial_t\chi = c\,\vec{\sigma}\cdot\vec{p}\,\phi + mc^2\,\chi, \tag{A3}$$

$$i\hbar\,\partial_t\phi = c\,\vec{\sigma}\cdot\vec{p}\,\chi - mc^2\,\phi, \tag{A4}$$

and the current density $\vec{J}_{\text{Dirac}} = c\left(\chi^\dagger\,\vec{\sigma}\,\phi + \phi^\dagger\,\vec{\sigma}\,\chi\right)$. Assuming energies near the rest mass $E = \mathcal{E} + mc^2$ and $\mathcal{E} \ll mc^2$, and solving in Eq. (A4) for the *small* component

$$\phi = \frac{c\,\vec{\sigma}\cdot\vec{p}}{E + mc^2}\,\chi \approx \frac{\vec{\sigma}\cdot\vec{p}}{2mc}\,\chi. \tag{A5}$$

one arrives, in the non-relativistic limit, at the time-independent Pauli equation for the *large* component

$$\mathcal{E}\,\chi = \frac{(\vec{\sigma}\cdot\vec{p})^2}{2m}\,\chi, \tag{A6}$$

where $\hat{H} = (\vec{\sigma}\cdot\vec{p})^2/2m$ is the Pauli Hamiltonian.

Appendix B: Boundary Conditions and Momentum Quantization

In the experimental setting, the space is finite, thus it is helpful to apply periodic boundary conditions in order to study the degeneracy of the allowed levels and safely compute numerical derivatives. We consider a rectangular region of dimensions $L_x \times L_y$. Because of our gauge selection, the eigenstates behave as plane waves in the y-direction. Hence, we apply periodic boundary conditions along this axis, while imposing strict physical limits on the x-direction. This can be summarized as:

$$\begin{cases} \chi(x, y + L_y) = \chi(x, y) \\ x \in [0, L_x]. \end{cases} \tag{B1}$$

This effectively gives the spatial domain the topology of a cylinder. Applying the periodic condition to the plane wave part of our solution, e^{iky}, yields:

$$\exp\{ik(y + L_y)\} = \exp\{iky\} \implies e^{ikL_y} = 1. \tag{B2}$$

This directly quantizes the momentum k:

$$k = \frac{2\pi\ell}{L_y}, \quad \text{with} \quad \ell \in \mathbb{Z}. \tag{B3}$$

Now the values of momentum k are quantized. However, from our theoretical framework, we know that the center of the harmonic oscillator (x_k) depends on k:

$$x_k = \frac{\hbar k}{qB_z} - \frac{mE_x}{qB_z^2}. \tag{B4}$$

Since the system is confined ($x_k \in [0, L_x]$), we cannot displace the wave-function arbitrarily. This boundary imposes cut-off values for the integer ℓ. Defining the charge sign as $\xi = \text{sign}(q)$ and the characteristic velocity $v_0 = \omega_B\ell_B$, we can rewrite x_k algebraically as:

$$x_k = \xi\left[\ell_B^2 k - \ell_B\frac{v_d}{v_0}\right] = \xi\left[\ell_B^2\frac{2\pi\ell}{L_y} - \ell_B\frac{v_d}{v_0}\right]. \tag{B5}$$

Equating this to the boundaries of our spatial domain gives the limits for ℓ. Setting $x_k = 0$:

$$\xi\left[\ell_B^2\frac{2\pi\ell}{L_y} - \ell_B\frac{v_d}{v_0}\right] = 0 \implies \ell = \frac{L_y}{2\pi\ell_B}\frac{v_d}{v_0}. \tag{B6}$$

Setting $x_k = L_x$:

$$\xi\left[\ell_B^2\frac{2\pi\ell}{L_y} - \ell_B\frac{v_d}{v_0}\right] = L_x \implies \ell = \frac{L_y}{2\pi\ell_B}\left(\xi\frac{L_x}{\ell_B} + \frac{v_d}{v_0}\right). \tag{B7}$$

Depending on the sign of the charge (ξ), these limits correspond to either the maximum or the minimum allowed integer. We can express ℓ_{min} and ℓ_{max} formally using the floor function $\lfloor x \rfloor$ (or integer part $E(x)$):

$$\ell_{min} = \left\lfloor \frac{L_y}{2\pi\ell_B}\left[\frac{v_d}{v_0} + \min\left(0, \xi\frac{L_x}{\ell_B}\right)\right]\right\rfloor, \tag{B8}$$

$$\ell_{max} = \left\lfloor \frac{L_y}{2\pi\ell_B}\left[\frac{v_d}{v_0} + \max\left(0, \xi\frac{L_x}{\ell_B}\right)\right]\right\rfloor. \tag{B9}$$

Note that ℓ_{min} could be negative depending on the direction of the drift velocity v_d. Thus, the allowed values for the momentum k are strictly restricted to:

$$k = \frac{2\pi\ell}{L_y} \quad \text{with} \quad \ell \in \mathbb{Z} \quad / \quad \ell_{min} \le \ell \le \ell_{max}. \tag{B10}$$

With these limits, we can compute the total number of allowed k-states (the degeneracy of the Landau level):

$$N_y = \ell_{max} - \ell_{min} \approx \left\lfloor \frac{L_xL_y}{2\pi\ell_B^2} \right\rfloor. \tag{B11}$$

The analytical solutions obtained previously are still valid, but with these new restrictions on k. Thanks to this finite domain, the eigenstates are now square-integrable and normalizable. Furthermore, this periodic topology is what allows us to employ spectral methods based on the Fast Fourier Transform (FFT) for our numerical simulations. To prevent unphysical wrapping artifacts in the confined x-direction (where the wave-function at $x = L_x$ could interact with $x = 0$ due to the FFT periodicity), we embed the system in the soft-wall potential V_{well} introduced in the numerical results section. This ensures the wave-function smoothly decays to zero well before reaching the transverse boundaries.

Appendix C: Exact Cancellation of the Bulk Current in the Ground State

1. Generic Pauli Current for Hall Eigenstates

To explicitly derive the probability current density components presented in Eq. (9) from the general Pauli definition in Eq. (3), we start with a generic stationary eigenstate of the Hall system:

$$\chi_{n,\sigma,k}(x,y) = \begin{pmatrix} c_\uparrow \\ c_\downarrow \end{pmatrix} \psi_{n,k}(x) \frac{e^{iky}}{\sqrt{L_y}}. \tag{C1}$$

The probability density is purely dependent on the x-coordinate, $|\chi|^2 = |\psi_{n,k}(x)|^2/L_y$.
The Pauli current consists of an orbital term and a spin term. The orbital contribution is given by:

$$\mathbf{J}_{\text{orb}} = \frac{1}{m}\text{Re}\left\{\chi^\dagger(\hat{\mathbf{p}} - q\mathbf{A})\chi\right\}. \tag{C2}$$

Applying the momentum operator $\hat{\mathbf{p}} = -i\hbar\nabla$, the x-component yields a purely imaginary value, which vanishes upon taking the real part. For the y-component, the derivative acts on the plane-wave phase e^{iky}, pulling down a factor of $\hbar k$. Using the Landau gauge $\mathbf{A} = (0, B_z x, 0)$, the orbital current naturally flows only in the y-direction:

$$\mathbf{J}_{\text{orb}} = \frac{\hbar k - qB_z x}{m}|\chi|^2\hat{\jmath}. \tag{C3}$$

The spin contribution to the current is defined as the curl of the spin magnetization:

$$\mathbf{J}_{\text{spin}} = \frac{\hbar}{2m}\nabla \times (\chi^\dagger \boldsymbol{\sigma}\chi). \tag{C4}$$

Since the state is an eigenstate of σ_z with eigenvalue $\sigma = \pm 1$, the inner product simplifies to a vector pointing purely in the z-direction: $\chi^\dagger\boldsymbol{\sigma}\chi = \sigma|\chi|^2\hat{k}$. Computing the curl of this vector field, where $|\chi|^2$ depends only on x, yields:

$$\nabla \times (\sigma|\chi|^2\hat{k}) = -\sigma\partial_x(|\chi|^2)\hat{\jmath}. \tag{C5}$$

By noting that $\partial_x|\chi|^2 = |\chi|^2\partial_x \ln|\chi|^2$, we arrive at the general spin current expression:

$$\mathbf{J}_{\text{spin}} = -\sigma\frac{\hbar}{2m}(\partial_x \ln|\chi|^2)|\chi|^2\hat{\jmath}. \tag{C6}$$

Combining both terms and implicitly assuming the charge sign in the cyclotron frequency definition, we recover the generic Hall current of Eq. (9).

2. Exact Cancellation in the Ground State

To explicitly see the exact local cancellation of the bulk current, we particularize this generic result to the ground state ($n = 0$) and carefully track the charge sign $q = \xi|q|$, with $\xi = \text{sgn}(q) = \pm 1$. We use the dimensionless shifted coordinate $\tilde{x} = (x - x_k)/\ell_B$, where $\ell_B = \sqrt{\hbar/m\omega_B}$.
For the lowest Landau level, the probability density is a Gaussian:

$$|\chi|^2 \propto \exp(-\tilde{x}^2), \tag{C7}$$

which implies $\partial_x \ln|\chi|^2 = \partial_x(-\tilde{x}^2) = -2\tilde{x}/\ell_B$. The spin current thus becomes:

$$\mathbf{J}_{\text{spin}} = \sigma\frac{\hbar}{m\ell_B}\tilde{x}|\chi|^2\hat{\jmath}. \tag{C8}$$

For the orbital term, using $|q|B_z = m\omega_B = \hbar/\ell_B^2$ (so $qB_z x = \xi\frac{\hbar}{\ell_B^2}x$), we rewrite the position as $x = x_k + \ell_B\tilde{x}$. The orbital current becomes:

$$\mathbf{J}_{\text{orb}} = \frac{\hbar}{m}\left[k - \xi\frac{x_k}{\ell_B^2} - \xi\frac{\tilde{x}}{\ell_B}\right]|\chi|^2\hat{\jmath}. \tag{C9}$$

Adding both contributions, the total probability current is:

$$\mathbf{J}_{\text{tot}} = \frac{\hbar}{m}\left[k - \xi\frac{x_k}{\ell_B^2} + \frac{(\sigma - \xi)}{\ell_B}\tilde{x}\right]|\chi|^2\hat{\jmath}. \tag{C10}$$

We clearly see that the spatially varying, $\tilde{x}$-dependent shear part cancels locally if and only if $\sigma = \xi$ (i.e., the spin polarization aligns with the sign of the charge). In this case:

$$\mathbf{J}_{\text{tot}}\Big|_{\sigma=\xi} = \frac{\hbar}{m}\left[k - \xi\frac{x_k}{\ell_B^2}\right]|\chi|^2\hat{\jmath}. \tag{C11}$$

Substituting the equilibrium position $x_k = \xi\ell_B^2(k - mE_x/\hbar B_z)$ from Eq. (7), the momentum k exactly cancels out, reducing the net current purely to the macroscopic drift:

$$\mathbf{J}_{\text{tot}} = \frac{E_x}{B_z}|\chi|^2\hat{\jmath} = v_d|\chi|^2\hat{\jmath}. \tag{C12}$$

This confirms that the topological cancellation perfectly shields the local density gradients, allowing the non-interacting condensate to strictly follow the classical $\mathbf{E} \times \mathbf{B}$ Hall drift.

[1] H. C. Ohanian, American Journal of Physics **54**, 500 (1986).
[2] M. Nowakowski, American Journal of Physics **67**, 916 (1999).
[3] Y.-J. Lin, R. L. Compton, K. Jiménez-García, J. V. Porto, and I. B. Spielman, Nature **462**, 628 (2009).
[4] J. J. Sakurai and J. Napolitano, *Modern Quantum Mechanics*, revised edition ed. (Addison-Wesley, San Francisco, 2011) Chap. 8, section 2.
[5] M. Abramowitz and I. A. Stegun, *Handbook of mathematical functions with formulas, graphs, and mathematical tables*, Vol. 55 (US Government printing office, 1948).
[6] L. D. Landau and E. M. Lifshitz, *Quantum mechanics: non-relativistic theory*, Vol. 3 (Elsevier, 2013).
[7] W. Bao and Q. Du, SIAM Journal on Scientific Computing **25**, 1674 (2004).
[8] S. Weinberg, *The quantum theory of fields*, Vol. 2 (Cambridge University Press, 1995).